



ELSEVIER

Available online at www.sciencedirect.com

SCIENCE @ DIRECT®

Earth and Planetary Science Letters 226 (2004) 367–382

EPSL

www.elsevier.com/locate/epsl

Fine-scale segmentation of volcanic/hydrothermal systems along fast-spreading ridge crests

Rachel M. Haymon^{a,*}, Scott M. White^b

^a*Department of Geological Sciences and Marine Science Institute, University of California, Santa Barbara, Santa Barbara, CA 93106, USA*

^b*Department of Geological Sciences, University of South Carolina, Columbia, SC 29205, USA*

Received 27 April 2004; received in revised form 9 July 2004; accepted 5 August 2004

Available online 11 September 2004

Editor: K. Farley

Abstract

Fine-scale (3rd and 4th order) segments of the mid-ocean ridge (MOR) are morphologically defined units of crustal accretion with enigmatic origins. At fast-spreading centers, 3rd order segments are bounded by discontinuities in the structure of the axial high. Most 3rd order segments are 20 ± 10 km long, and terminate at ridge axis discontinuities (RADs) exhibiting 0.2–3 km lateral offsets and/or ≥ 20 m axial depth increases. Nested within 3rd order segments are shorter 4th order segments bounded by smaller RADs. Along the fast-spreading East Pacific Rise (EPR) at $10^{\circ}02' - 9^{\circ}08' \text{ N}$ and $17^{\circ}11' - 42' \text{ S}$, spatial distributions of active high-temperature hydrothermal vents, biological communities, and lava flow morphology are known accurately from extensive near-bottom surveys and submersible dives along a total of seven 3rd order segments and twenty-four 4th order segments. The cumulative northern and southern EPR data show that 3rd order segments (but not 4th order segments) consistently exhibit apparently higher rates of lava effusion near segment middles in comparison to segment ends, supporting the hypothesis that each 3rd order segment is a discrete, centrally fed volcanic system, or “volcanic segment”. Spatial analyses of the cumulative hydrothermal data reveal a striking increase in abundance of hydrothermal features within the middle portions of 3rd order segments. Approximately 60% of ongoing high-temperature focused flow is concentrated within the middle 40% of 3rd order segments, and twice as many biological communities are found at mid-segment in comparison to segment ends. The two independent data sets—volcanic and hydrothermal—both indicate that magmatic heat sources are focused beneath the central portions of 3rd order segments, and that magmatic/hydrothermal systems are spatially and temporally segmented at 3rd order length and time scales. We propose that 3rd order segmentation arises from processes controlling melt supply to the middle-to-lower crust; and, that 4th order segmentation largely arises from more rapid/frequent upper crust processes of crack formation and dike intrusion. Future work is needed to test the applicability of our results along portions of the fast-

* Corresponding author. Tel.: +1 805 893 3718; fax: +1 805 893 2314.

E-mail address: haymon@geol.ucsb.edu (R.M. Haymon).

spreading EPR notched by fault-bounded axial troughs, and in areas farther south where spreading rate reaches a maximum.

© 2004 Elsevier B.V. All rights reserved.

Keywords: mid-ocean ridge; ridge segmentation; volcanic segments; hydrothermal vents; lava flow morphology; East Pacific Rise; fast-spreading ridges; Argo

1. Introduction

In response to the discontinuous and episodic nature of cracking and magma supply along divergent plate boundaries, the global mid-ocean ridge system (MOR) is comprised of many spreading segments operating over a range of lengths (10^0 – 10^3 km) and time scales (10^1 – 10^7 years) (see [1] and references therein). The smallest ridge segments are nuclei for the accretion of unit blocks of ocean crust, and are influencing seafloor creation in ways that are not fully understood. The origins and evolution of these fine-scale segments are enigmatic because there are not many places where spatial resolution and extent of sonar data permit them to be distinguished and studied, and also because fine-scale segments are too short-lived (10^5 years or less) to leave a magnetic anomaly record on the ridge flanks. However, since seafloor volcanic and hydrothermal features are observable manifestations of crustal accretion, the distributions of these features reveal how magmatic and hydrothermal systems along the ridge crest are behaving, and illuminate the nature of fine-scale ridge segments. We therefore examine here the distributions of volcanic and hydrothermal features along fine-scale segments of the fast-spreading East Pacific Rise (EPR).

The MOR crest is partitioned into fine-scale segments by small depth anomalies and/or lateral offsets of the ridge axis. On fast-spreading ridges, axis depth anomalies that are not associated with obvious lateral offset of the ridge axis are referred to as saddles, or as “small non-overlapping offsets” (SNOOS) [2], while small lateral ridge axis offsets are called “deviations from axial linearity” (“Devals”) [3]. In the hierarchy of ridge segments described by Macdonald et al. [1,4], fine-scale segment boundaries are subdivided into “3rd or 4th order ridge axis discontinuities” (RADs). 3rd order RADs on fast-spreading ridges are discontinuities of the axial high manifested as saddles along the ridge crest with axial depth increases of ≥ 20 m, and/or

as lateral axis offsets of 0.2–3 km. These are the smallest RADs that can be detected from the sea surface with 12 kHz multibeam sonar systems. 4th order RADs offset the ridge axis by less than 200 m, hence high resolution near-bottom sonar systems are required to detect them, and to distinguish them from small 3rd order RADs [5,6] (Fig. 1).

Currently, there are only two places where both the spatial distributions of discrete seafloor hydrothermal and volcanic features and the locations of fine-scale ridge segment boundaries have been thoroughly mapped. These two areas are located along the EPR (Fig. 1), where full spreading rates are ≥ 11 cm/year.

2. Previous work

2.1. Origin of morphological/structural segmentation of the EPR

The nature of ridge segmentation along the EPR has been studied by many investigators (e.g., [1–16] and references therein). Macdonald et al. [1,4] originally suggested that 1st and 2nd order ridge segments, bounded by transform faults and overlapping spreading centers (OSCs), are underlain by separate axial magma chambers, and speculated that smaller 3rd order and 4th order segments might arise either from pinching, jogs, or multiple convection cells along a single, continuous magma chamber; or, alternatively, by feeding of magma to the seafloor along dikes that produce, or follow, discontinuous, en echelon crack systems.

Because some fine-scale RADs show a change between segments in the compositions of erupted lava flows, Langmuir et al. [3] postulated that constrictions or obstructions to magma mixing in the axial magma chamber must occur at fine-scale RADs, and argued that fine-scale segmentation originates at the level of axial magma chambers.

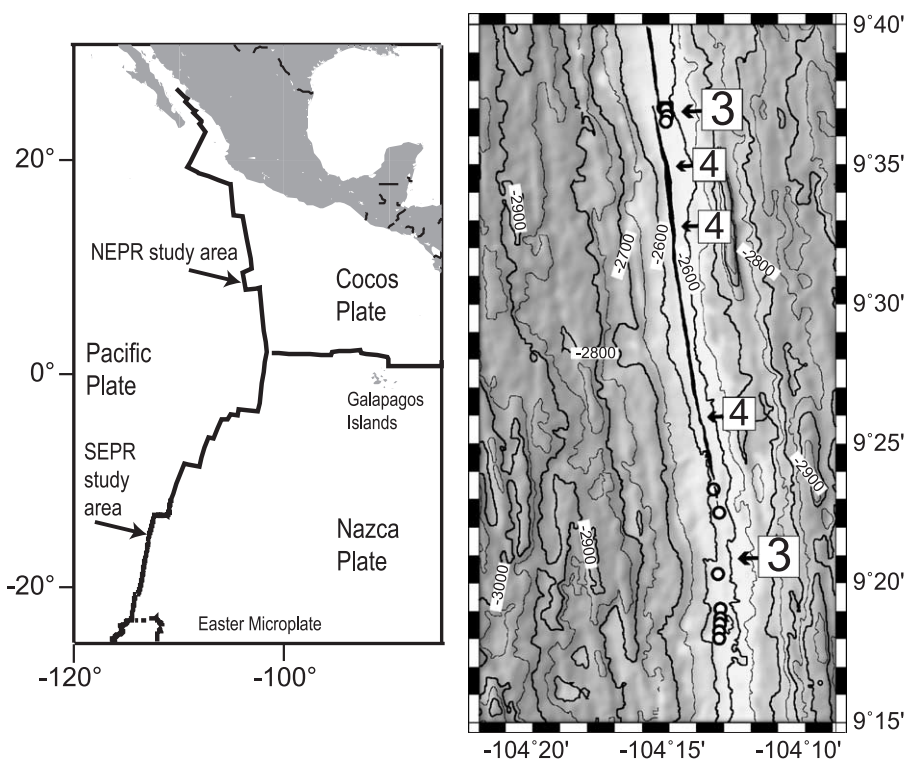


Fig. 1. Left panel shows locations of NEPR and SEPR near-bottom surveys. Right panel shows contoured, shaded-relief bathymetry map of the EPR crest at 9°40'–15' N (contour interval=50 m). The axial summit collapse trough [5,26] is outlined in black, and open circles denote locations of volcanic domes (constructional pillow mounds) along the ridge crest [18]. The area shown encompasses a complete 3rd order segment with nested 4th order segments; segment boundaries are ridge axis discontinuities (RADs) labeled “3” (3rd order) and “4” (4th order). 3rd order RADs are discontinuities in the axial high, expressed as either ≥ 20 m axial depth increases at saddle points, or 0.2–3 km lateral axis offsets; 3rd order RADs are marked by clusters of volcanic domes. 4th order RADs are discontinuities of the axial zone, manifested as either terminations, or < 0.2 km lateral offsets, in linear axial features (e.g., axial troughs, fissure systems, or volcanic constructions); no clusters of volcanic domes are associated with 4th order RADs.

However, not all fine-scale segment boundaries along the EPR are also geochemical boundaries [16]. Noting this, and observing along the EPR crest at 9–10°N that numerous 5–15-km-long segments are bounded by lateral offsets, or abrupt changes, in the types of features which are created by magma delivery to the neovolcanic zone (such as collapsed lava ponds, fissures, and axial lava flows of different relative ages), Haymon et al. [5] proposed that most of the smallest-scale ridge segments are created by shallow intrusions of individual dikes or dike swarms.

Seismic imaging beneath the EPR crest reveals local pinching and discontinuities of crustal low velocity zones at wavelengths matching that of fine-scale segmentation, lending support to the idea that

many fine-scale segments correspond to segmentation of axial magma chambers [9,14]. In addition, along-strike changes in seismic properties of the crustal melt sill beneath the southern EPR axis, attributed to variations in crystal/melt ratios, are observed at the length scale of fine-scale segmentation [10]; however, since the locations of fine-scale RADs along this portion of the southern EPR are unmapped, it is unknown if there is a direct spatial correspondence between morphologic ridge segmentation and these possible changes in crystal/melt ratios. Recently, imaging of the seismic velocity structure of the upper mantle beneath the EPR at 9–10°N has revealed 3rd order length scale (~20 km) modulations suggesting possible subcrustal origin of 3rd order segmentation [17].

2.2. Volcanic segmentation of the EPR

White et al. used near bottom DSL-120 kHz sonar data to distinguish 3rd order from 4th order segments on the southern EPR from 18°30' to 17°15' S [6] and on the northern EPR from 9°08' to 10°N [18]. Once this distinction was made, a consistent distribution of volcanic features along 3rd order segments was evident: specifically, more sheet flows and volcanic collapses were found near segment middles, and more pillowed flows and small lava domes were found near segment ends (Figs. 1 and 2). From this distribution of volcanic features, White et al. inferred that 3rd order segments consistently show a change along strike from higher effusion rates (and/or lower lava viscosities) near segment middles to lower effusion rates (and/or higher lava viscosities) near segment ends.

The inference that effusion rates are highest at mid-segment is consistent with the idea that 3rd order segments on the EPR are behaving individually as centrally fed, elongate, very low-relief volcanic systems, or “volcanic segments”, that are typically 20 ± 10 km in length and persist for 10^3 – 10^5 years [6,18]. This establishes a clear and very significant distinction between the characteristics of 3rd order segments and those of 4th order segments. 4th order segments are shorter in length (7 ± 5 km) and duration ($< 10^3$ years) than 3rd order segments, and vary from segment to segment in volcanic characteristics and apparent effusion rates, rather than exhibiting the consistent middle-to-end reduction in inferred effusion rates shown by 3rd order segments (Fig. 3).

2.3. Hydrothermal segmentation of the EPR

Hydrothermal systems respond to the thermal structure of the MOR (which is strongly influenced by magma supply, storage, and delivery), and to the permeability field (which is strongly influenced by fracturing). If morphologic and structural segmentation of the ridge arises from the spatially and temporally discontinuous way in which the plate boundary cracks apart and is fed with magma, then it is reasonable to hypothesize that hydrothermal systems are correspondingly segmented. Observations suggesting this linkage between morphological/structural ridge segmentation and segmentation of ridge crest hydrothermal activity were made initially

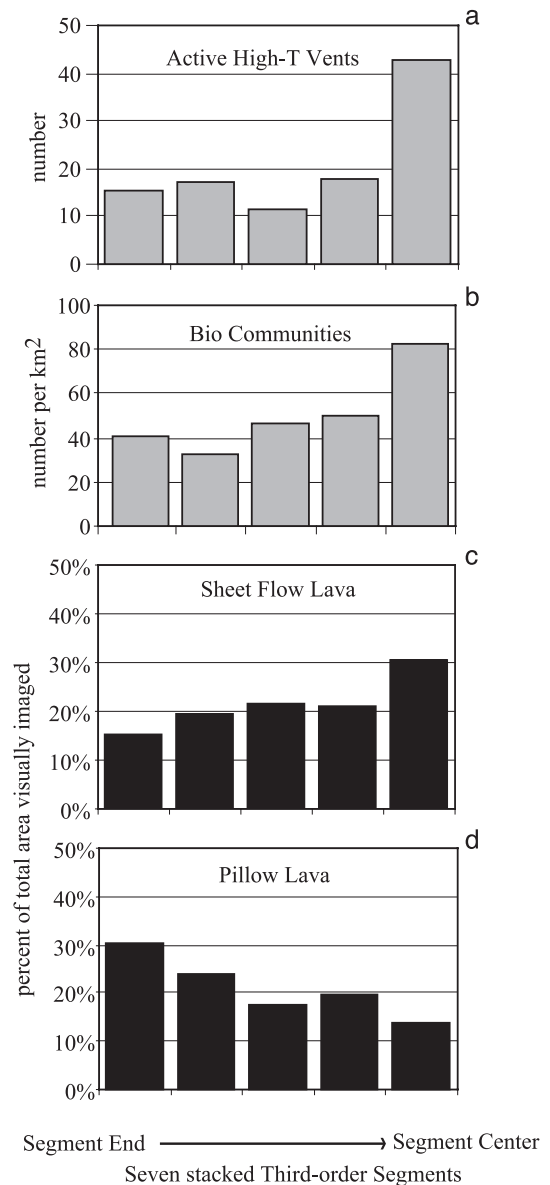


Fig. 2. Composite NEPR and SEPR 3rd order histograms showing (a) increase in active high-*T* chimneys (top plot), (b) increase in biological communities (upper middle plot), (c) increase in sheet flows (lower middle plot), and (d) decrease in pillows (bottom plot), from segment end (left) to middle (right). Data from seven 3rd order segments were normalized to correct for variations in segment length, and stacked into cumulative plots. Note: ~60% of all active high-*T* vents cluster in the middle two bins that correspond to the middle 40% of 3rd order segments.

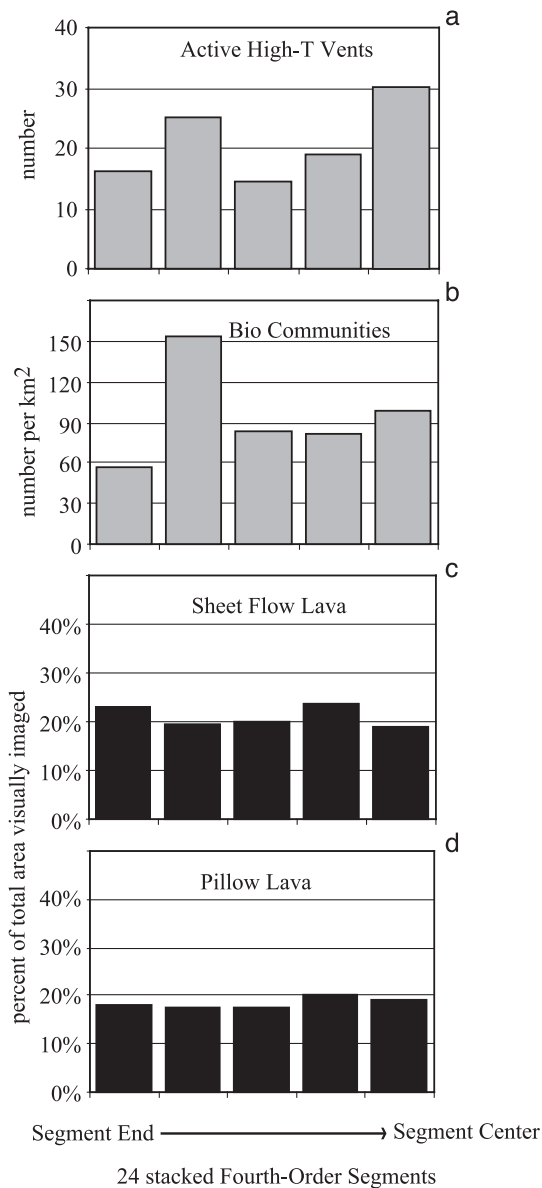


Fig. 3. Composite NEPR and SEPR 4th order histograms showing essentially random distribution from segment end (left) to segment middle (right) in (a) active high- T chimneys (top plot), (b) biological communities (upper middle plot), (c) sheet flows (lower middle plot), and (d) pillows (bottom plot). Data from twenty-four 4th order segments were normalized to correct for variations in segment length, and stacked into cumulative plots.

when near-bottom imaging with the Argo I system was used to identify both fine-scale segment boundaries and the distribution of hydrothermal vents

along the EPR at $9^{\circ}08' - 54' \text{ N}$ [5,19,20]. Continuous near-bottom imaging of the axial zone along strike revealed where vents were currently active, and, just as importantly, showed where hydrothermal activity was sparse. These data allowed spatial patterns of hydrothermal activity along the ridge to be discerned and compared with morphologic/structural segmentation of the ridge.

For the large-scale 2nd order segment bounded by the Clipperton Transform and the $9^{\circ}03' \text{ N}$ OSC, the majority of active hydrothermal vents are found along the shallowest, north-central portion of the segment (Fig. 4), and numbers of vents decline toward both ends of the segment (though no Argo I coverage of the distal segment tips was obtained). Haymon et al. [5] interpreted this mid-segment concentration of active vents as evidence that a persistent enhanced magma supply near the center of the 2nd order segment provides a sustained heat source to power hydrothermal vents.

Subsequent regional-scale hydrothermal plume studies along multiple fast-spreading 2nd order segments of the EPR have revealed a consistent tendency for higher plume incidence and intensity above the relatively inflated middle portions of segments compared to their (typically) deflated ends [21,22]. The plume observations compellingly support the idea that magma supply to the EPR is greatest near mid-segment [1], and that magma supply is the primary control on the distribution of hydrothermal vents along the EPR at a 2nd order scale [5,19,21,22].

Because no clear criteria existed in 1989 for distinguishing small 3rd order RADs from 4th order RADs, and because the EPR $9-10^{\circ} \text{ N}$ Argo I sonar data were collected too near the seafloor for detection of the abundant lava domes that characterize 3rd order RADs (Fig. 1; [6,18]), all of the fine-scale segments observed in the Argo I sonar records were considered to be 4th order segments on the basis of their small lateral offsets [5]. Hence, the distribution of volcanic and hydrothermal features with respect to 3rd order vs. 4th order segments was not previously investigated.

Near-bottom DSL-120 kHz sonar and Argo II photographic surveys along the ultrafast-spreading southern EPR were conducted in late 1996 [23] to test the general applicability to fast-spreading ridges

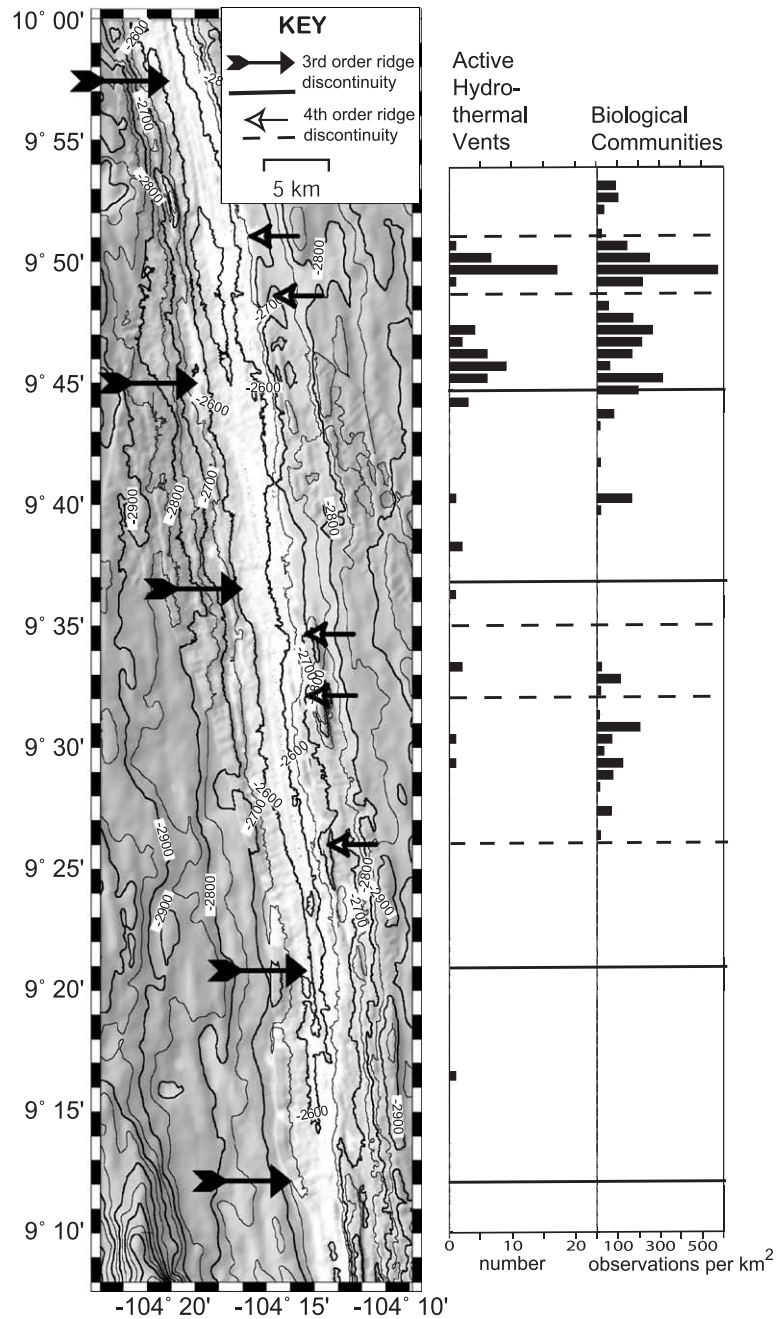


Fig. 4. *Left panel*: NEPR contoured, shaded-relief bathymetry map with segment boundaries (RADs) shown (contour interval=50 m). RADs typically are zones of overlap along-strike between two adjacent segments. Filled arrows on left point to midpoints of 3rd order RAD zones; open-headed arrows on right point to midpoints of 4th order RAD zones. *Right panel*: histograms (binned at 0.5' latitude intervals) showing along-strike distributions of active high- T vents and biological communities; 3rd order RAD midpoints are denoted by solid lines, 4th order RAD midpoints are denoted by dashed lines. Note that gaps or minima in hydrothermal features occur at 3rd order RADs.

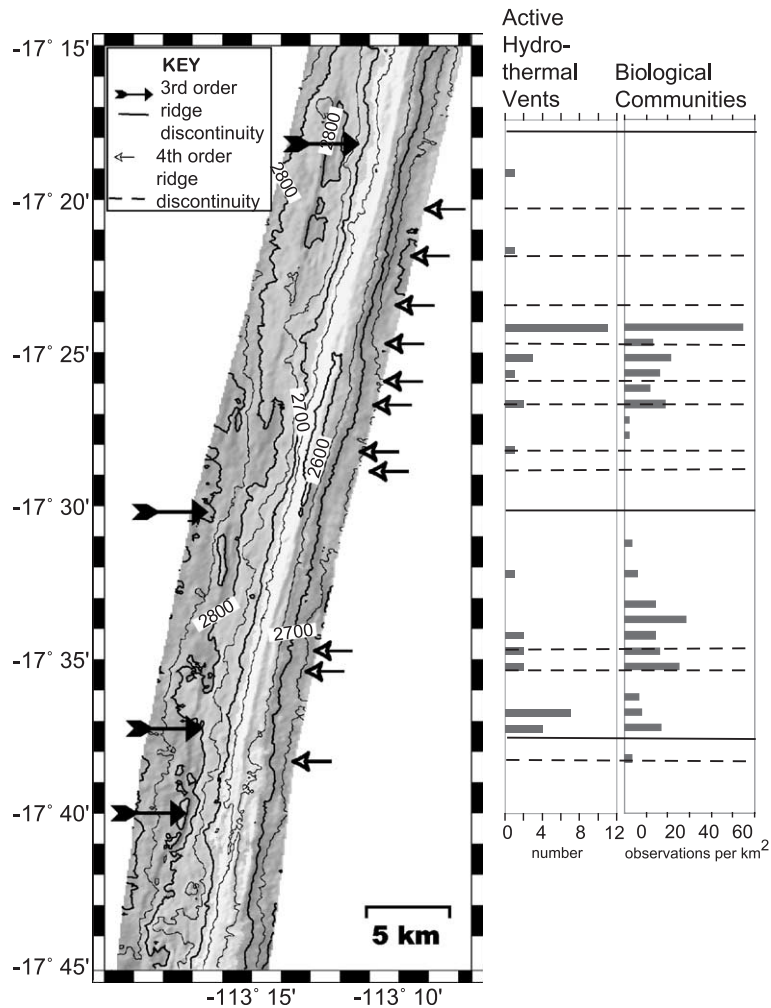


Fig. 5. *Left panel*: SEPR contoured, shaded-relief bathymetry map with segment boundaries (RADs) shown (contour interval=50 m). RADs typically are zones of overlap along-strike between two adjacent segments. Filled arrows on left point to midpoints of 3rd order RAD zones; open-headed arrows on right point to midpoints of 4th order RAD zones. *Right panel*: histograms (binned at 0.5' latitude intervals) showing along-strike distributions of active high- T vents and biological communities; 3rd order RAD midpoints are denoted by solid lines, 4th order RAD midpoints are denoted by dashed lines. Note that gaps or minima in hydrothermal features occur at 3rd order RADs.

of segmentation hypotheses arising from observations at EPR 9–10°N. The survey data along the southern EPR indicate clear segment-to-segment changes in the abundance and maturity of hydrothermal vents, axial lava age, and fissure density across large 3rd order RADs, i.e., across RADs visible in multibeam bathymetry as small OSCs [23]. However, such changes between segments are much less obvious across smaller 3rd and 4th order RADs on the southern EPR (Fig. 5).

3. Objectives and methods

3.1. Objectives

If 3rd order segments really are individual volcanic systems with magma supply focused in the middles of segments, as proposed by White et al. [6,18], then hydrothermal vents should be more abundant in the middles of 3rd order segments where heat sources are concentrated. The current study was undertaken to test

this hypothesis, and to compare hydrothermal vent distribution on 3rd vs. 4th order EPR segments.

We have conducted quantitative statistical analyses of hydrothermal feature distribution along all of the 3rd and 4th order segments within both of the EPR Argo survey areas. These analyses take advantage of the clear delineation of 3rd vs. 4th order segment boundaries in the two survey areas, and of an analytical approach (described below) that allows data from multiple segments to be stacked so that the signal of overall trends emerges from the noise of individual segment data distributions [6,18].

3.2. Features used as indices of hydrothermal activity

During the EPR Argo surveys, we identified locations of (1) active chimneys (mineral structures that were visibly emitting fluids), and (2) biological communities. Active chimneys are sites of focused, high-temperature fluid discharge, and indicate where there presently is sufficient heat to permit metals and sulfide to be transported to the seafloor. Biological communities occur in areas of active fluid flow, and disclose the presence of low-level hydrothermal activity at sites where fluid flow may be too diffuse to be optically detectable. When fluid flow ceases altogether, these animals quickly disappear.

3.3. Methods of data collection

Most of the hydrothermal observations in this study were made from seafloor video collected during two dense, strike-continuous Argo surveys along the EPR crest (Fig. 1). We collected data with coaxial Argo I in 1989 along an 83-km portion of the fast-spreading northern EPR (NEPR) axial zone from 9°09' N to 9°54' N [5]. In 1996, fiber-optic Argo II was used to collect data along a 45-km portion of the ultrafast-spreading southern EPR (SEPR) axial zone from 17°11' S to 17°40' S [23–25]. In both survey areas, the axial zone is <200 m wide in most places [5,6,26].

Both Argo surveys were highly successful in locating and describing the hydrothermal activity within their respective areas. Photographic coverage throughout these areas is 15–25% within a 1-km-wide neovolcanic zone, and typically >40% within 100 m of the ridge axis. The placement of each successive Argo line relied on the observations from previous

lines, in that previous observations of distal smoke plumes and fields of animals were used to home in on the locations of active high-temperature vents. Argo vehicle navigation precision is ≤ 5 m within the global navigational coordinate system [5,26]; therefore, we could navigate well enough to locate active chimneys based on the coordinates of features seen on previous lines. The success of this search method in finding almost all of the active high-temperature sites within the axial zone, as well as the accuracy and precision of the Argo vent locations, was verified by submersible programs within the two survey areas [27–33]. Divers were able to locate quickly the hydrothermal features found with Argo, and discovered new active high-temperature sites mainly at EPR 9°45'–52' N, where a post-Argo eruption perturbed the hydrothermal system in 1991–1992 [27–29].

Thus for our statistical study, which combines all vents found by Argo and/or by submersible, we have confidence that almost all of the focused, high-temperature vents active within the Argo survey areas in 1989–1998 were located (Table 1), even though <100% of the ridge crest was visually imaged during the surveys.

During the NEPR Argo survey, vents were distinguished by their geographic coordinates, and active chimneys were described as black smokers (BSM), white smokers (WSM), or grey smokers (GSM). During the SEPR Argo survey, vents were numbered (e.g., “SP-20”). These generic Argo vent designators are used in Table 1 for vents that do not have other unique names; however, at sites where vents located with Argo have been given more distinctive names during submersible programs, these “dive names” are provided in Table 1 in place of Argo vent labels. Sites where vents were located both by Argo and by submersible are indicated by asterisks in Table 1. From this annotation, it is clear that outside the 1991–1992 NEPR eruption area (where new vents were spawned by an eruption after the 1989 Argo survey) only three sites of known high-temperature flow were undetected with Argo (R Vent; Soupape; and Moxa).

3.4. Methods of counting features

Our data analysis procedure looks primarily at the along-axis distribution patterns of discrete hydrothermal features within the Argo survey areas relative to the 3rd and 4th order segment boundaries established by

previous work (Table 2). Since the density of coverage and style of video observations were similar on both surveys, and since differences in image quality between

Table 1
Active high-*T* hydrothermal vents (1989–1998)

Vent site designator	Longitude	Latitude	Number of vents
<i>NEPR</i>			
<i>BioVent</i>	−104°17.6′	9°51.0′	1
<i>N</i>	−104°17.6′	9°50.9′	1
<i>M</i>	−104°17.6′	9°50.8′	1
<i>Q</i>	−104°17.6′	9°50.8′	1
<i>G (Tica)**</i>	−104°17.5′	9°50.4′	1
<i>WSM</i>	−104°17.5′	9°50.4′	7
<i>Bio9** and P**</i>	−104°17.5′	9°50.3′	5
<i>BSM</i>	−104°17.5′	9°50.3′	3
<i>Damocles Sword, Ty, Io</i>	−104°17.5′	9°50.2′	3
<i>TWP*</i>	−104°17.3′	9°49.6′	1
<i>WSM</i>	−104°17.0′	9°47.5′	4
<i>V</i>	−104°17.0′	9°47.3′	1
<i>GSM</i>	−104°17.0′	9°47.2′	1
<i>T</i>	−104°16.9′	9°46.8′	1
<i>A and J</i>	−104°16.8′	9°46.6′	4
<i>GSM</i>	−104°16.8′	9°46.5′	1
<i>L*</i>	−104°16.7′	9°46.3′	9
<i>BSM</i>	−104°16.6′	9°45.6′	1
<i>WSM</i>	−104°16.6′	9°45.6′	4
<i>GSM</i>	−104°16.6′	9°45.5′	1
<i>BSM</i>	−104°16.5′	9°44.9′	2
<i>H*</i>	−104°15.9′	9°40.9′	1
<i>B* and C*</i>	−104°15.5′	9°38.9′	2
<i>R</i>	−104°15.5′	9°36.8′	1
<i>D* and E*</i>	−104°14.9′	9°33.5′	2
<i>K*</i>	−104°14.5′	9°29.7′	1
<i>F*</i>	−104°13.1′	9°16.8′	1
<i>SEPR</i>			
<i>SP20</i>	−113°10.6′	−17°19.6′	1
<i>Soupape</i>	−113°11.4′	−17°22.4′	1
<i>SP25C/Stanley*</i>	−113°12.0′	−17°24.6′	2
<i>SP25W/Le Chat (N. Smoker)*</i>	−113°12.2′	−17°24.9′	4
<i>Rehu-Marka*</i>	−113°12.2′	−17°24.9′	5
<i>SP26/Nadir/S. Smoker*</i>	−113°12.4′	−17°25.9′	3
<i>Moxa</i>	−113°12.4′	−17°26.2′	1
<i>Gumbo*</i>	−113°12.6′	−17°27.0′	1
<i>Dumbo*</i>	−113°12.8′	−17°27.4′	1
<i>SP29</i>	−113°13.1′	−17°28.9′	1
<i>Spike/Wormwood/ Hobbes/Suzie*</i>	−113°14.8′	−17°35.5′	4
<i>SP36/Calvin*</i>	−113°14.9′	−17°35.8′	2
<i>SP37E “Stealth Smokers”/ Homer/Marge*</i>	−113°15.1′	−17°37.2′	7
<i>Bart*</i>	−113°15.3′	−17°37.6′	1
<i>SP38/Wally/Maggie*</i>	−113°15.3′	−17°37.8′	3

Argo I and Argo II video systems are unimportant to the gross counts of features we examine in this study, we can directly compare results from the two surveys.

On crossing Argo lines, the same active chimney may be observed more than once. To exclude duplicate observations of a single active chimney from our database, we compared the coordinates of each chimney to the coordinates of all other chimneys in the database. Duplicate observations, i.e., those whose locations matched that of another chimney within the precision of our navigation (within ± 5 m), were eliminated from the database. Submersible observations [23,28] and Argo photomosaics [25] also were used to improve the accuracy of chimney counts at sites where multiple, closely spaced active chimneys were present.

We define a biological community as an observation of five or more individual animals within the field-of-view of the Argo downlooking video camera. This corresponds to a spatial density of at least one animal per 5 m². To mitigate the effect of multiple observations of the same area on closely spaced or crossing Argo lines, the location of each observation was projected onto a 5-m grid so that a maximum of one observation (recorded as presence or absence of five or more animals) was allowed for each 5-m² area of seafloor imaged by Argo.

The amount of seafloor visually imaged with Argo varies along strike. We do not need to account for this in plotting the distribution of active hydrothermal chimneys, since relatively few focused flow vents exist and virtually all were well located by the Argo

Notes to Table 1:

Active high-*T* sites observed with Argo only denoted as: BSM=black smoker; GSM=grey smoker; WSM=white smoker (NEPR); or “SP” (SEPR).

Some Argo sites were never investigated by submersible (e.g., near 9°45′ N).

Italics denote NEPR sites that lie within the 1991–1992 eruption area [4]. Except for some new vents spawned post-Argo by the 1991–1992 NEPR eruption, almost all other known vents on the NEPR and SEPR were detected with Argo.

Data sources: NEPR vents [5,26,27,28,29]; SEPR vents [24,25,30,31,32].

* Active high-*T* vent areas identified by Argo, also found and named by divers.

** New active high-*T* vents found by submersible within 1991 eruption area, located very close to high-*T* vents found in 1989 with Argo.

Table 2
Ridge axis discontinuities (RADs) bounding ridge segments in EPR study areas

Order	Latitude of RAD	Name of segment north of RAD	RAD description
<i>NEPR</i>			
3	9°57' N	–	Saddle (20 m); axis azimuth change
4	9°51.5' N	A	North tip of axial summit trough (AST)
4	9°49' N	B1	Right step of AST (~50 m)
3	9°44.8' N	B2	Right step of AST (relay zone ~0.5 km)
3	9°37' N	C	Right step of AST (~0.5 km)
4	9°34.9' N	D	Right step of axis (~100 m); AST widens
4	9°32.7' N	E1	Right step of AST (~60 m)
4	9°26.1' N	E2	Southern tip of well-defined AST
3	9°21' N	F	Right step of ridge axis (0.5–1 km)
3	9°12' N	G	Right step of ridge axis (~0.5 km)
<i>SEPR</i>			
3	17°18.5' S	–	Saddle (20 m)
4	17°20.35' S	Cold 1	Left step of ridge axis (~100 m)
4	17°21.75' S	Cold 2	Right step of ridge axis (<100 m)
4	17°23.5' S	Cold 3	Right step of ridge axis (<100 m)
4	17°24.7' S	Cold 4	Right step of ridge axis (~100 m)
4	17°26' S	Apex	North tip of AST (“Aldo Lake”)
4	17°26.75' S	Aldo 1	Right step of AST (~125 m)
4	17°28.2' S	Aldo 2	Left step of AST (~75 m)
4	17°29' S	Aldo 3	South tip of AST
3	17°30' S	Aldo 4	Left step of ridge axis (~0.2 km)
4	17°33.75' S	Tubeworm 1	Left steps of axis (relay zone ~75 m)
4	17°34.5' S	Tubeworm 2	Left steps of axis (relay zone ~75 m)
3	17°36' S	Tubeworm 3	Left step of ridge axis (~0.2 km)
4	17°37.25' S	Stealth 1	Right step of ridge axis (~120 m)
3	17°40' S	Stealth 2	Saddle (30 m); axis right step (<100 m)

surveys. However, raw counts of biological communities, which have a more widespread and less fully known distribution, could be biased by variations along-strike in the area of seafloor imaged. To remove this bias in the histograms presented, we calculated the area of Argo coverage within each bin and converted the raw observation counts in each bin to the number of observations per km².

3.5. Methods of data analysis

We present the hydrothermal data in two ways to compare to segmentation. One familiar way presents the data along-strike by latitude, because the EPR runs approximately north–south in both study areas (Figs. 4 and 5). We present the data as histograms of feature counts binned by latitude, with a 0.5' (~1 km) bin width. The advantage of this presentation is that the distribution of features around a particular location is clear. However, overall patterns are more difficult to judge since the traits of individual areas are so apparent and distracting.

An alternate presentation method is one in which the data are normalized to segment length and then stacked. The two Argo survey areas combined include seven 3rd order segments and twenty-four 4th order segments (Table 2). For each 3rd and 4th order segment, we normalize the distribution of hydrothermal features to segment length by calculating the distance from the feature to the nearest segment end, then dividing by half of the segment length. The normalized values for locations of features along a segment thus range from 0 (at segment end) to 1 (at mid-segment). After normalizing the data to segment length, all of the observations for both survey areas are stacked into cumulative middle-to-end (half-segment) 3rd order and 4th order plots (Figs. 2 and 3).

This method of plotting has great advantages for presenting the patterns of feature distribution within segments. Stacking segments overcomes the distracting variation inherent in all natural processes, enhancing the signal/noise ratio so that what is

Notes to Table 2:

Data sources: NEPR 4th order segment boundaries and names [5]; NEPR 3rd order segment boundaries [18]; SEPR 4th order segment boundaries and names [23,24]; SEPR 3rd order segment boundaries [6]. Axial summit trough denoted as “AST”.

average or typical can emerge. The stacking method thus permits us to recognize and compare the overall patterns that define the respective distributions of hydrothermal activity and volcanic flow morphology for 3rd and 4th order EPR ridge segments. Because there are segment-to-segment variations in hydrothermal vent abundances, it is inevitable that the more active segments will dominate the overall signal in our stacked plots. We do not consider this to be a sampling bias; rather, it is a true averaging of the temporal signal embedded in our spatial distribution of vents. By adding together segments from both the NEPR and SEPR survey areas, we think we have included enough segments in different stages of activity to obtain a time-averaged spatial distribution signal.

The choice of bin width along strike is somewhat arbitrary. The relatively small number ($n < 65$) of active high-temperature chimneys in each of our study areas suggests that 10 bins per full (end-to-end) segment is appropriate. This corresponds to along-axis bin widths of 2 ± 1 km for 3rd order segments, and 700 ± 500 m for 4th order segments, and allows each bin to be wide enough to reduce random noise, but narrow enough to reveal patterns that exist. When the segments are halved from middle-to-end and the data are stacked into cumulative histograms (Figs. 2 and 3), each of the five bins in the half-segment histograms represents 20% of total segment length. These bin widths should be sufficient to show any trends within the stacked, segment length-normalized graphs.

4. Results

4.1. Distributions of hydrothermal features and lava flow morphology along 3rd order segments

Plots of the distribution of hydrothermal features along-strike by latitude are shown in Figs. 4 (NEPR) and 5 (SEPR). Note that RADs often are regions of overlap between the tips of adjacent offset ridge segments; the ratio of overlap distance: offset distance is typically $\sim 3:1$ [4]. The arrows in Figs. 4 and 5 point either to sharp discontinuities, or to the midpoints of RAD overlap zones. A salient feature of these plots is the gap or minima in counts of hydrothermal features that is typically observed at 3rd order RADs. These gaps suggest that ridge crest hydrothermal systems are

discontinuous along-strike and may be segmented at the 3rd order scale. One can also see in these plots that some 3rd order segments are more hydrothermally active than others, as discussed previously.

The cumulative, segment-length normalized and stacked distributions of hydrothermal features and volcanic flow morphology for all 3rd order (NEPR+SEPR) segments are shown in Fig. 2. The plots in Fig. 2 show that average abundances of active chimneys are strongly skewed toward the centers of 3rd order segments. Approximately 60% of ongoing high-temperature focused flow is concentrated within the two middle bins, i.e., within the middle 40% of 3rd order segments. Furthermore, twice as many biological communities occur in the mid-segment bin in comparison to the end-segment bin. Thus, both indicators for active fluid flow (focused and diffuse) provide evidence that hydrothermal vents are most prolific within the central 40% portions of 3rd order segments (where the ratio of sheet flows to pillowed flows is highest) and decrease in abundance towards the ends of these segments (where the ratio of sheet flows to pillowed flows is least). If the ratio of sheet to pillowed flows is an accurate indicator of relative effusion rates, such that higher ratios correspond to relatively higher effusion rates, then the data in Fig. 2 indicate enhanced heat sources producing effusive eruptions and powering hydrothermal vents near the middles of 3rd order ridge segments.

4.2. Distributions of hydrothermal features and lava flow morphology along 4th order segments

Fig. 3 shows cumulative, segment-length normalized and stacked distributions of hydrothermal features for all 4th order (NEPR+SEPR) segments. Unlike 3rd order segments, the plots in Fig. 3 show that average distributions of active hydrothermal features and lava flow types essentially are random along the lengths of 4th order segments.

Thus 4th order segments do not show the middle-to-end declines in hydrothermal vent abundance and apparent lava effusion rates that are exhibited by 3rd order segments. Instead, segment-to-segment variations in hydrothermal vent abundance and distribution along 4th order segments, observable in Figs. 4 and 5, sum to produce the random distribution with respect to distance along the segment shown in Fig. 3.

Although active vents within the 1991 eruption area ($9^{\circ}52' - 45' \text{ N}$) tend to be located near the centers of 4th order segments (Fig. 4), vents found on older lava flows along 4th order segments in the southern part of the NEPR survey area (Fig. 4), and along 4th order SEPR segments (Fig. 5), do not show this trend, suggesting that the mid-4th order segment vent clustering within the 1991 eruption area is either coincidental or highly transient.

5. Discussion

5.1. Origins of fine-scale segmentation on fast-spreading ridges

Reductions in apparent lava effusion rates at segment ends theoretically can be caused either by enhanced hydrothermal cooling, or by decreased magma supply at segment ends. If enhanced hydrothermal cooling were to blame, then hydrothermal vent abundance would be expected to increase at segment ends—this is in fact opposite to what is observed. The robust, systematic along-strike increases observed in both hydrothermal vent abundance and apparent lava effusion rates towards the middles of 3rd order segments are entirely consistent with the following: (1) magma supply to middle/lower crust reservoirs along the EPR is organized at 3rd order length and time scales and focused toward segment centers, providing a persistent mid-segment source of magma and heat; (2) EPR hydrothermal systems are coupled to 3rd order segmentation of magma supply.

Although crustal permeability is an important control on hydrothermal vent distribution, particularly along portions of the MOR that are magmatically quiescent, we consider it to be secondary to magma supply in both of our magmatically active EPR study areas. In both areas, hydrothermal vents are most abundant on recent lava flows in sparsely fissured sheet flow terrain [5,20,24], and the vast majority of vents are located along eruptive and noneruptive fissures above dike intrusions [20,24,25,27,28,34]. This is true where axial summit collapse troughs are present ($9^{\circ}51.5 - 26.1' \text{ N}$, $17^{\circ}29 - 26' \text{ S}$), and where they are not present ($9^{\circ}21 - 12' \text{ N}$, $17^{\circ}18.5 - 26' \text{ S}$, $17^{\circ}26 - 40' \text{ S}$). Clearly, it is the feeding of magma to the seafloor from crustal reservoirs that is producing

most of the permeability pathways and hydrothermal vents that we observe.

Fig. 6 depicts a conceptual model for 3rd order EPR segmentation that is consistent with both the hydrothermal and volcanic data. In this model, 3rd order segments are analogous to elongate low-relief volcanic systems with a centralized magma supply. Hydrothermal activity declines along strike from the central “summit” region, where high magma supply produces effusive sheet flows and collapsed lava ponds, to the periphery of the volcanic system where reduced magma supply produces less effusive pillowed flows and constructional mounds.

A 3rd order EPR segment usually hosts at least two 4th order segments (this is illustrated in Fig. 6, where a 4th order RAD divides a 3rd order segment into two 4th order segments). 4th order segments conceivably can be created by a variety of upper crustal processes. Clearly, many EPR 4th order segments containing axial troughs are spawned by eruptive dike intrusions [5,20,28,35]. Others possibly originate from fissuring above non-eruptive dikes, or by amagmatic tectonic cracking. 4th order segments may form individually from discrete dike intrusion or fissuring events; or, as an echelon sets of segments developed in concert above/along a single propagating dike or crack. Random distribution of hydrothermal and volcanic features along 4th order segments may be an expression of a diversity in mechanisms that give rise to 4th order segments; or, alternatively, may be an indication that 4th order segments arise from short-lived events that exert only transient control on hydrothermal vent distribution, and exert no control on rates of lava effusion.

Recently, Cormier et al. [35] and Carbotte et al. [36] have described a cycle of magmatic inflation and subsidence of the EPR axial high that occurs on a 3rd order time scale ($10^3 - 10^4$ years) [35], and may be caused by small (3–4%) mismatches between rates of magma replenishment of axial magma reservoirs and rates of magma withdrawal by dike intrusion [36]. These studies are consistent with our proposed origin of 3rd order segments from spatial/temporal variations in magma supply to the middle/lower crust, and of 4th order segments from dike intrusion and cracking in the upper crust.

Both of the EPR Argo surveys used in our study were conducted on portions of the EPR that lack large, fault-bounded axial troughs, and both are in the

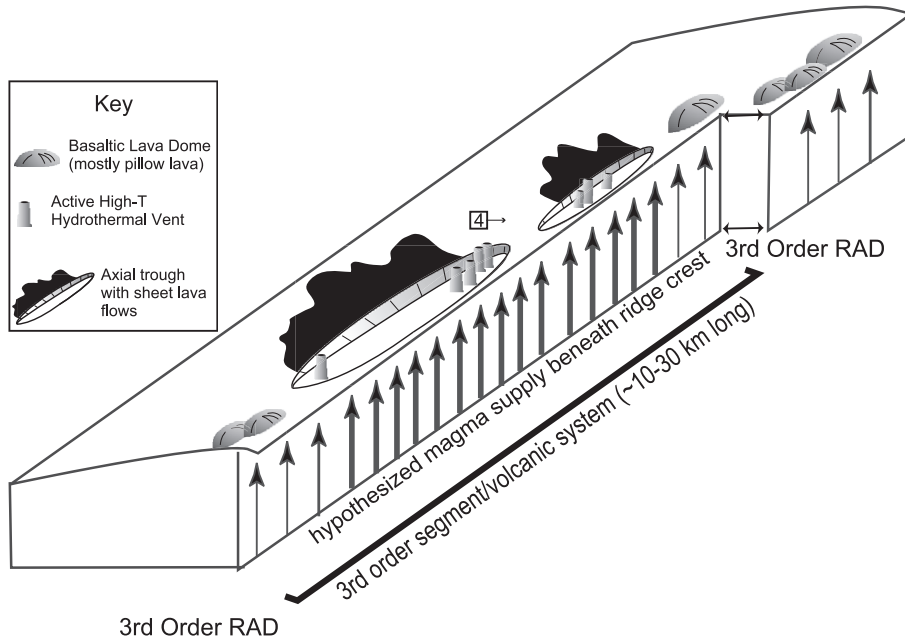


Fig. 6. 3D sketch of fast-spreading ridge crest segmented at 3rd and 4th order scales: a single 3rd order segment, divided by a 4th order RAD into two 4th order segments, is illustrated here. Chimney icons illustrate distribution of high- T vents; vertical arrows illustrate magma supply (bold arrows indicate more robust magma supply at mid-segment, lighter weight arrows indicate diminution in magma supply near segment ends).

inflated, “waxing” stage described by Cormier et al. [35] in which small, volcanic axial collapse troughs sometimes form. Hence, Fig. 6 is a depiction of a 3rd order segment in the “waxing” stage of evolution. Because we used a method of stacking data to enhance the signal present in inherently noisy volcanic and hydrothermal data, it is advantageous that both survey areas are on “waxing” portions of the EPR, and thus have comparable patterns of hydrothermal activity and magma supply that are unaffected by the added complexity of permeability effects on hydrothermal circulation introduced by ridge crest faults that may form during the “waning” stage [35,36]. Since our study areas do include multiple segments with and without unfaulted, volcanic axial collapse troughs, our study should be fully representative of “waxing” fast-spreading ridge crests.

5.2. Implications for EPR hydrothermal systems

4th order segments persist for short periods of time (decades to millennia) relative to 3rd order segments (millennia to 10^5 years). These time scales are

consistent with the relative rapidity of 4th order crack and dike propagation in comparison to 3rd order magmatic inflation and deflation of the axial high. The distribution of 4th order segment boundaries and hydrothermal vents will be reconfigured many times (probably tens to hundreds of times) during the life span of a 3rd order segment. 4th order events can cause short-term temporal variations in hydrothermal flow, and can shift locations of hydrothermal seafloor vents, but the data show that on average the majority of vents remain clustered in the midsections of 3rd order segments.

Recent work along a 610-km-long portion of the ultrafast-spreading southern EPR crest has shown a robust spatial correlation between hydrothermal plume intensity, cross-sectional area of the axial high (binned at 3-km intervals) [22], and areas of flat-lying sheet flows [37]. These results suggest that hydrothermal vent distribution is governed by heat supply, and they are generally consistent with our findings that hydrothermal vents cluster in ~ 3 – 10 -km-long central portions of 3rd order volcanic segments where apparent effusion rates indicate maxima in magma

supply. However, at maximum spreading rates there may be some differences in patterns of dike and crack propagation, overall fracture patterns, and distribution of heat sources that produce some deviations from segment-centered distribution of hydrothermal vents and effusive volcanism such as we describe [37]. This possibility remains to be tested.

In a previous study of hydrothermal plume intensity variations along the northern EPR at 15°20′–18°30′ N, Baker et al. [38] suggested that formation of a small fault-bounded rift valley plays an important role in enhancing axial hydrothermal discharge. Because the areas of the EPR that we studied are both in the “waxing” stage (discussed above), we do not assess here the impact that ridge crest faults at the margins of axial troughs or rift valleys might have on distribution of hydrothermal vents with respect to segment boundaries.

6. Conclusions

Spatial analysis of active hydrothermal chimney and biological community distribution with respect to the boundaries of seven 3rd order and twenty-four 4th order segments on the EPR reveals:

- (1) striking concentration of hydrothermal activity in the middle portions of 3rd order segments (60% of hydrothermal vents occur in the middle 40% of 3rd order segments);
- (2) spatial coincidence in the middles of 3rd order segments between increased numbers of hydrothermal vents and increased numbers of volcanic features indicative of high lava effusion rates (sheet flows; collapse structures);
- (3) random distribution of hydrothermal and volcanic features along 4th order segments.

We conclude from these observations that:

- (1) magma feeding eruptions and heat powering hydrothermal vents are focused toward the middles of 3rd order segments;
- (2) 3rd order segments are essentially discrete volcanic/hydrothermal systems typically spaced at 20 ± 10 -km intervals along the EPR, and lasting thousands to hundreds of thousands of years;

- (3) 3rd order segments originate from the processes that supply magma to axial magma reservoirs in the middle-to-lower crust;
- (4) 4th order segments arise from shallower cracking, dike intrusion, and delivery of magma to the upper crust and seafloor;
- (5) 4th order processes reconfigure 4th order segment boundaries and hydrothermal vent distribution, and perturb hydrothermal flow, many times during the life span of a 3rd order volcanic system, but on average the majority of vents remain clustered in the midsections of 3rd order segments.

Acknowledgements

We would like to thank all the captains, crews, WHOI techs, and scientists on the Venture III (R/V *T. Washington*), Sojourn II (R/V *Melville*), and AHA-NEMO (R/V *Melville*) research expeditions, who assisted in collecting sonar and photographic data used in this research. Special thanks go to Joanna Hobson O’Neill for her post-cruise assistance in compiling the SEPR hydrothermal vents data, and to Brooke Stenbridge for her assistance in digitizing lava morphology data. We express our profound thanks to Ken Macdonald for much helpful discussion, and for his review of an early draft of the manuscript. We greatly appreciate thoughtful reviews of the submitted manuscript provided by Ed Baker and Dick Hey. Thanks also to Dawn Wright, Suzanne Carbotte, Milene Cormier, and Dan Scheirer for their help at sea and for their scientific insights into causes of segmentation. Milene Cormier also gave us helpful information about SEPR vents visited during the 1993 Naudur dives. This research was supported by National Science Foundation Grants OCE88-17587 (RMH) and OCE94-16996 (RMH). Partial support for Scott White was provided by OCE98-16021 (to Ken Macdonald).

References

- [1] K.C. Macdonald, P.J. Fox, L.J. Perram, M.F. Eisen, R.M. Haymon, S.P. Miller, S.M. Carbotte, M.-H. Cormier, A.N. Shor, A new view of the mid-ocean ridge from the behaviour of ridge-axis discontinuities, *Nature* 335 (1988) 217–225.

- [2] R. Batiza, S.H. Margolis, A model for the origin of small non-overlapping offsets (SNOOs) of the East Pacific Rise, *Nature* 320 (1986) 439–441.
- [3] C.H. Langmuir, J.F. Bender, R. Batiza, Petrological and tectonic segmentation of the East Pacific Rise, 5°30' N–14°30' N, *Nature* 322 (1986) 422–429.
- [4] K. Macdonald, J.-C. Sempere, P.J. Fox, East Pacific Rise from Siqueiros to Orozco Fracture Zones: along-strike continuity of axial neovolcanic zone and structure and evolution of overlapping spreading centers, *J. Geophys. Res.* 89 (1984) 6049–6069.
- [5] R.M. Haymon, D.J. Fornari, M.H. Edwards, S. Carbotte, D. Wright, K.C. Macdonald, Hydrothermal vent distribution along the East Pacific Rise Crest (9°09'–54' N) and its relationship to magmatic and tectonic processes on fast-spreading mid-ocean ridges, *Earth Planet. Sci. Lett.* 104 (1991) 513–534.
- [6] S.M. White, K.C. Macdonald, R.M. Haymon, Basaltic lava domes, lava lakes, and volcanic segmentation on the southern East Pacific Rise, *J. Geophys. Res.* 105 (2000) 23519–23536.
- [7] K.C. Macdonald, Linkages between faulting, volcanism, hydrothermal activity and segmentation on fast-spreading centers, in: W.R. Buck, P.A. Delaney, J.A. Karson, Y. Lagabriele (Eds.), *Faulting and Magmatism at Mid-Ocean Ridges*, Geophysical Monograph, vol. 106, 348, American Geophysical Union, Washington, DC, 1998, pp. 27–59.
- [8] P. Lonsdale, Segmentation of the Pacific-Nazca spreading center, 1°N–20°S, *J. Geophys. Res.* 94 (1989) 12197–12226.
- [9] D.R. Toomey, S.C. Solomon, G.M. Purdy, Tomographic imaging of the shallow crustal structure of the East Pacific Rise at 9°30' N, *J. Geophys. Res.* 99 (1994) 24135–24157.
- [10] S.C. Singh, G.M. Kent, J.S. Collier, A.J. Harding, J.A. Orcutt, Melt to mush variations in crustal magma properties along the ridge crest at the southern East Pacific Rise, *Nature* 394 (1998) 874–878.
- [11] G.M. Kent, S.C. Singh, A.J. Harding, M.C. Sinha, J.A. Orcutt, P.J. Barton, R.S. White, S. Bazin, R.W. Hobbs, C.H. Tong, J.W. Pye, Evidence from three-dimensional seismic reflectivity images for enhanced melt supply beneath mid-ocean ridge discontinuities, *Nature* 406 (2000) 406–414.
- [12] R.A. Dunn, D.R. Toomey, R.S. Detrick, W.S.D. Wilcock, Continuous mantle melt supply beneath an overlapping spreading center on the East Pacific Rise, *Science* 291 (2001) 1955–1958.
- [13] J.P. Canales, R.S. Detrick, D.R. Toomey, W.S.D. Wilcock, Segment-scale variations in the crustal structure of 150–300 kyr old fast spreading oceanic crust (East Pacific Rise, 8°15' N–10°5' N) from wide-angle seismic refraction profiles, *Geophys. J. Int.* 152 (2003) 766–794.
- [14] S.M. Carbotte, G. Ponce-Correa, A. Solomon, Evaluation of morphological indicators of magma supply and segmentation from a seismic reflection study of the EPR 15°30'–17°N, *J. Geophys. Res.* 105 (2000) 2737–2759.
- [15] J. Sinton, R. Detrick, J.P. Canales, G. Ito, M. Behn, Morphology and segmentation of the western Galapagos Spreading Center, 90.5°–98°W: plume–ridge interaction at an intermediate spreading ridge, *Geochem., Geophys., Geosys.* 4 (2003) 1–26.
- [16] J.M. Sinton, S.M. Smaglik, J.J. Mahoney, K.C. Macdonald, Magmatic processes at superfast spreading mid-ocean ridges: glass compositional variations along the East Pacific Rise 13°–23°S, *J. Geophys. Res.* 96 (1991) 6133–6155.
- [17] D.R. Toomey, R.A. Dunn, W.S.D. Wilcock, R.S. Detrick, Mantle structure beneath the East Pacific Rise and its relation to tectonic segmentation, axial morphology, and hydrothermal activity, *EOS, Trans. Am. Geophys. Union* 84 (2003) F224–F225.
- [18] S.M. White, R.M. Haymon, D.J. Fornari, M.R. Perfit, K.C. Macdonald, Correlation between volcanic and tectonic segmentation of fast-spreading ridges: evidence from volcanic structures and lava flow morphology on the East Pacific Rise at 9°–10°N, *J. Geophys. Res.* 107 (2002) 2173–2192.
- [19] R. Haymon, The response of ridge-crest hydrothermal systems to segmented, episodic magma supply, in: C.J. MacLeod, P.A. Tyler, C.L. Walker (Eds.), *Tectonic, Magmatic, Hydrothermal and Biological Segmentation of Mid-Ocean Ridges*, 118, Geological Society, London, 1996, pp. 157–168, Special Publication.
- [20] D.J. Wright, R.M. Haymon, D.J. Fornari, Crustal fissuring and its relationship to magmatic and hydrothermal processes on the East Pacific Rise crest (9°12' to 54' N), *J. Geophys. Res.* 100 (1995) 6097–6120.
- [21] E.T. Baker, Geological indexes of hydrothermal venting, *J. Geophys. Res.* 101 (B6) (1996) 13741–13753.
- [22] E.T. Baker, R.N. Hey, J.E. Lupton, J.A. Resing, R.A. Feely, J.J. Gharib, G.J. Massoth, F.J. Sansone, M. Kleinrock, F. Martinez, D.F. Naar, C. Rodrigo, D. Bohnenstiehl, D. Pardee, Hydrothermal venting along earth's fastest spreading center: East Pacific Rise, 27.5°–32.3°S, *J. Geophys. Res.* 107 (2002) 1–19.
- [23] R.M. Haymon, K.C. Macdonald, S. Baron, L. Crowder, J. Hobson, P. Sharfstein, S. White, B. Bezy, E. Birk, F. Terra, D. Scheirer, D. Wright, L. Magde, C.V. Dover, S. Sudarikov, G. Levai, Distribution of fine-scale hydrothermal, volcanic, and tectonic features along the EPR crest, 17°15'–18°30' S: results of near-bottom acoustic and optical surveys, *Eos Trans. Am. Geophys. Union* 78 (46) (1997) F705.
- [24] D.J. Wright, R.M. Haymon, S.M. White, K.C. Macdonald, Crustal fissuring on the crest of the southern East Pacific Rise at 17°15'–40' S, *J. Geophys. Res.* 107 (2002) 5-1–5-13.
- [25] J.M.H. O'Neill, Geologic controls on distribution of hydrothermal vents on the superfast-spreading southern EPR, Master's Thesis, U.C. Santa Barbara, 1998.
- [26] D.J. Fornari, R.M. Haymon, M.R. Perfit, T.K.P. Gregg, M. Edwards, Axial summit caldera of the East Pacific Rise 9°–10°N: geologic characteristics and evolution of the axial zone on fast-spreading mid-ocean ridges, *J. Geophys. Res.* 103 (1998) 9827–9856.
- [27] T.M. Shank, D.J. Fornari, K.L. von Damm, M.D. Lilley, R.M. Haymon, R.A. Lutz, Temporal and spatial patterns of biological community development at nascent deep-sea hydrothermal vents (9°50' N, East Pacific Rise), *Deep-Sea Res., Part II, Top. Stud. Oceanogr.* 45 (1998) 465–515.

- [28] R.M. Haymon, D.J. Fornari, K.L.V. Damm, M.D. Lilley, M.R. Perfit, J.M. Edmond, W.C. Shanks III, R.A. Lutz, J.M. Grebmeier, S. Carbotte, D. Wright, E. McLaughlin, M. Smith, N. Beedle, E. Olson, Volcanic eruption of the mid-ocean ridge along the East Pacific Rise crest at 9° 45–52' N: direct submersible observations of seafloor phenomena associated with an eruption event in April, 1991, *Earth Planet. Sci. Lett.* 118, 85–101 (1993).
- [29] K.L. Von Damm, Chemistry of hydrothermal vent fluids from 9–10°N, East Pacific Rise: “Time Zero” the immediate post-eruptive period, *J. Geophys. Res.* 105 (2000) 11203–11222.
- [30] M. Lilley, E.J. Olson, G.K. Proskurowski, A.W. Graham, Volatiles in vent fluids from the southern East Pacific Rise, *EOS, Trans. Amer. Geophys. Union* 80 (1999) F1099.
- [31] J.-M. Auzende, V. Ballu, R. Batiza, D. Bideau, J.-L. Charlou, M.-H. Cormier, Y. Fouquet, P. Geistdoerfer, Y. Lagabriele, J. Sinton, P. Spadea, Recent tectonic, magmatic, and hydrothermal activity on the East Pacific Rise between 17°S and 19°S: submersible observations, *J. Geophys. Res.* 101 (1996) 17995–18010.
- [32] R.W. Embley, J.E. Lupton, G. Massoth, T. Urabe, V. Tunnicliffe, D.A. Butterfield, T. Shibata, O. Okano, M. Kinoshita, K. Fujioka, Geologic, chemical, and biological evidence for recent volcanism at 17.5°S, East Pacific Rise, *Earth Planet. Sci. Lett.* 163 (1998) 131–147.
- [33] J. Sinton, E. Bergmanis, K. Rubin, R. Batiza, T.K.P. Gregg, K. Gronvold, K. Macdonald, S. White, Volcanic eruptions on mid-ocean ridges: new evidence from the superfast-spreading East Pacific Rise, 17°–19°S, *J. Geophys. Res.* 107 (2002) 2115–2130.
- [34] D.J. Wright, R.M. Haymon, K.C. Macdonald, Breaking new ground: estimates of crack depth along the axial zone of the East Pacific Rise (9°12'–54' N), *Earth Planet. Sci. Lett.* 134 (1995) 441–457.
- [35] M.H. Cormier, W.B.F. Ryan, A.K. Shah, W. Jin, A. Bradley, D.R. Yoerger, Waxing and waning volcanism along the East Pacific Rise on a millenium time scale, *Geology* 31 (2003) 633–636.
- [36] S.M. Carbotte, W.B.F. Ryan, W. Jin, M.H. Cormier, E. Bergmanis, J. Sinton, S. White, Magmatic subsidence of the East Pacific Rise (EPR) at 18°14' S revealed through fault restoration of ridge crest bathymetry, *Geochem. Geophys. Geosyst.* 4 (1) (2003) 1–1–1–21.
- [37] R. Hey, E. Baker, D. Bohnenstiehl, G. Massoth, M. Kleinrock, F. Martinez, D. Naar, D. Pardee, J. Lupton, R. Feely, J. Gharib, J. Resing, C. Rodrigo, F. Sansone, S. Walker, Tectonic and volcanic segmentation and controls on hydrothermal venting along Earth's fastest active seafloor spreading system, EPR 27°–32°S, *Geochemistry, Geophysics, Geosystems*, submitted for publication.
- [38] E.T. Baker, M.H. Cormier, C.H. Langmuir, K. Zavala, Hydrothermal plumes along segments of contrasting magmatic influences, 15°20'–18°30' N, East Pacific Rise: influence of axial faulting, *Geochem. Geophys. Geosyst.* 2 (2001) 1–20.